Article

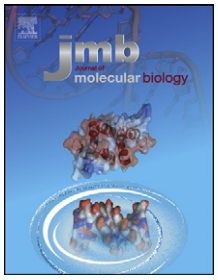

Intrinsic Disorder Mediates Cooperative Signal Transduction in STIM1

Yukio Furukawa[1,†], Shunsuke Teraguchi[2,3,†], Takahisa Ikegami[4], Onur Dagliyan[5], Lin Jin[6], Damien Hall[6,7], Nikolay V. Dokholyan[5], Keiichi Namba[1], Shizuo Akira[2], Tomohiro Kurosaki[8], Yoshihiro Baba[8] and Daron M. Standley[6]

1 - Nanobiology Laboratories, *Protonic NanoMachine Group, Graduate School of Frontier Biosciences, Osaka University, Osaka 565–0871, Japan*
2 - Laboratory of Host Defense, *WPI Immunology Frontier Research Center, Osaka University, Osaka 565–0871, Japan*
3 - Quantitative Immunology Research Unit, *WPI Immunology Frontier Research Center, Osaka University, Osaka 565–0871, Japan*
4 - Laboratory of Advanced Protein Characterization, *Research Center for State-of-the-Art Functional Protein Analysis, Institute for Protein Research, Osaka University, Osaka 565–0871, Japan*
5 - Department of Biochemistry and Biophysics, *School of Medicine, University of North Carolina at Chapel Hill, Chapel Hill, NC 27599, USA*
6 - Laboratory of Systems Immunology, *WPI Immunology Frontier Research Center, Osaka University, Osaka 565–0871, Japan*
7 - Research School of Chemistry, *Australian National University Section on Biophysical Chemistry, Acton, 0200 ACT, Australia*
8 - Laboratory of Lymphocyte Differentiation, *WPI Immunology Frontier Research Center, Osaka University, Osaka 565–0871, Japan*

Correspondence to Daron M. Standley: *standley@ifrec.osaka-u.ac.jp*
http://dx.doi.org/10.1016/j.jmb.2014.03.006
Edited by R. W. Kriwacki

Abstract

Intrinsically disordered domains have been reported to play important roles in signal transduction networks by introducing cooperativity into protein–protein interactions. Unlike intrinsically disordered domains that become ordered upon binding, the EF-SAM domain in the stromal interaction molecule (STIM) 1 is distinct in that it is ordered in the monomeric state and partially unfolded in its oligomeric state, with the population of the two states depending on the local Ca^{2+} concentration. The oligomerization of STIM1, which triggers extracellular Ca^{2+} influx, exhibits cooperativity with respect to the local endoplasmic reticulum Ca^{2+} concentration. Although the physiological importance of the oligomerization reaction is well established, the mechanism of the observed cooperativity is not known. Here, we examine the response of the STIM1 EF-SAM domain to changes in Ca^{2+} concentration using mathematical modeling based on *in vitro* experiments. We find that the EF-SAM domain partially unfolds and dimerizes cooperatively with respect to Ca^{2+} concentration, with Hill coefficients and half-maximal activation concentrations very close to the values observed *in vivo* for STIM1 redistribution and extracellular Ca^{2+} influx. Our mathematical model of the dimerization reaction agrees quantitatively with our analytical ultracentrifugation-based measurements and previously published free energies of unfolding. A simple interpretation of these results is that Ca^{2+} loss effectively acts as a denaturant, enabling cooperative dimerization and robust signal transduction. We present a structural model of the Ca^{2+}-unbound EF-SAM domain that is consistent with a wide range of evidence, including resistance to proteolytic cleavage of the putative dimerization portion.

© 2014 The Authors. Published by Elsevier Ltd. This is an open access article under the CC BY-NC-ND license (http://creativecommons.org/licenses/by-nc-nd/3.0/).

Introduction

It is well known that intrinsically disordered domains (IDDs) are common in eukaryotic proteins [1], in particular in protein–protein interaction (PPI) hubs [2]. The functional role of IDDs in PPIs has been explained in terms of versatility: their flexibility allows them to interact with multiple binding partners

0022-2836/$ - see front matter © 2014 The Authors. Published by Elsevier Ltd. This is an open access article under the CC BY-NC-ND license (http://creativecommons.org/licenses/by-nc-nd/3.0/).

[3]. In addition, since order/disorder reactions can be triggered by changes in the local chemical environment, phosphorylation, or ligand binding, IDDs play important roles as switches in signaling pathways [4]. Moreover, several recent studies [5–8] have shed light on another function of IDDs that underlies their role in PPIs: cooperativity. By folding upon binding, IDDs can mediate allosteric coupling between spatially distant domains. For example, the binding of tetracycline (Tc) to the Tc repressor (TetR) causes the dynamics of the intrinsically disordered DNA-binding domain to become strongly coupled to the more structured Tc binding/dimerization domains [8]. Another example of IDD-mediated cooperativity is the phd antitoxin of the phd/doc toxin–antitoxin operon, which is an extrachromosomal addiction module located on the P1 prophage and is responsible for the postsegregational killing effect (death of plasmid-free cells) of *Escherichia coli* [7]. The IDD in phd was shown to be stabilized by binding to doc, which, in turn, increased or decreased phd's affinity for its target DNA sequence, depending on the relative phd/doc ratio [7]. In a third example, the IDD-containing adenovirus protein E1A was shown to mediate either positive or negative cooperativity between host proteins TAZ2 and pRB, depending on the availability of E1A-binding sites [5]. More recently, ligand-dependent folding was found to regulate the activity of the homodimeric enzyme aminoglycoside *N-(6)-acetyltransferase-Ii* [6]. Interestingly, Hilser and Thompson showed earlier that an IDD in a multi-domain system could maximize allosteric coupling between ligand-binding sites [9]. The above are just four examples of such "IDD-mediated allostery", but the abundance of IDDs in signaling molecules and nuclear proteins suggests that there may be a greater link between intrinsic disorder and the cooperativity of intermolecular interactions than previously realized.

Here, we describe yet another variation on IDD-mediated cooperativity. In the examples above, the IDD in question becomes ordered upon ligand binding, and this ordering facilitates energetic coupling between spatially separated binding sites. In contrast, the endoplasmic reticulum (ER) luminal domain in the ER membrane-bound stromal interaction molecule (STIM) 1 equilibrates between a folded monomeric state and a

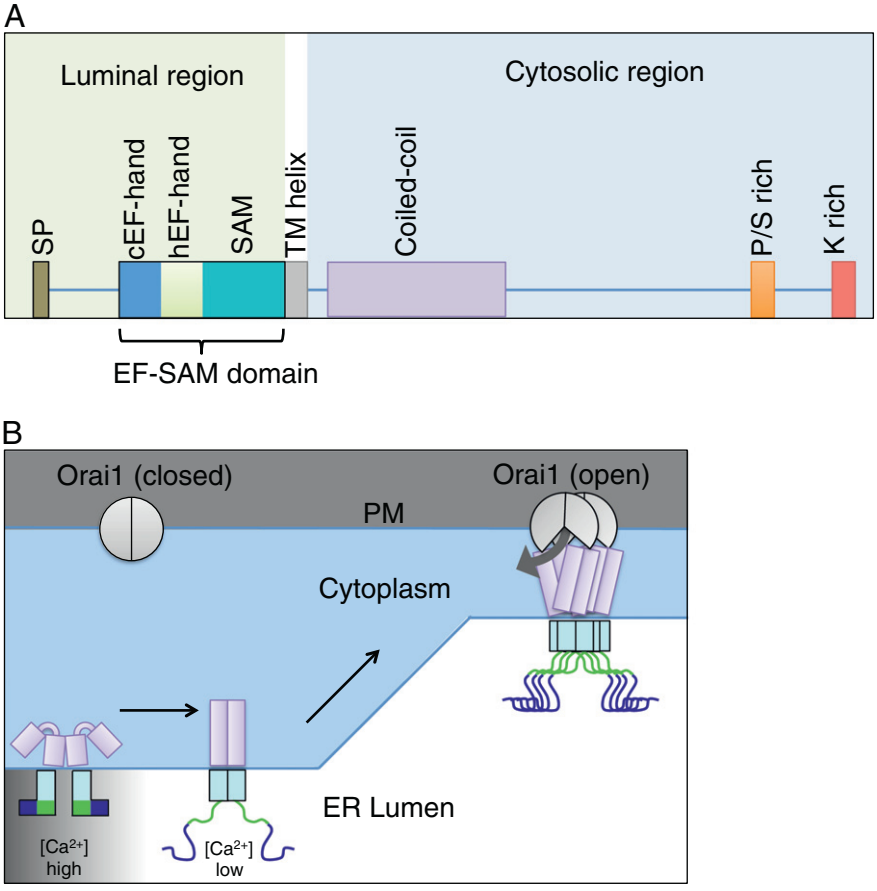

Fig. 1. Overview of STIM1 function. (A) Domain architectures of luminal and cytosolic regions are indicated to scale. (B) Schematic illustration of CRAC channel opening.

partially unfolded oligomeric state, with the population of the two states depending on the local calcium concentration. Such "conditional disorder" has been demonstrated previously in the case of stress-induced chaperones, which unfold upon loss of zinc binding [10]. STIM1 proteins play a critical role in store-operated Ca^{2+} entry (SOCE), a mechanism used by many cells, including immune cells, to increase intracellular Ca^{2+} concentrations, leading to the transmission of a wide variety of signals. Several studies in mice have indicated that SOCE is physiologically important in mast cells [11], T cells [12], B cells [13], and skeletal muscles [14]. Mutations in the *Stim1* gene typically result in severe combined immunodeficiency [15].

STIM1 contains a single-pass transmembrane helix that separates cytoplasmic and luminal regions (Fig. 1A). The luminal region contains a "canonical" Ca^{2+}-binding EF-hand motif (cEF-hand), a second "hidden" EF-hand motif (hEF-hand) that does not bind Ca^{2+}, and a sterile alpha motif (SAM) domain; collectively, these three luminal motifs are referred to as the "EF-SAM" domain [16]. When the luminal Ca^{2+} concentration is high, the EF-SAM domain is monomeric, and a solution structure of the monomeric, Ca^{2+}-bound EF-SAM domain has been determined [17]. The cytosolic region contains coiled-coil, proline/serine-rich, and lysine-rich regions, which are reported to dimerize in the resting state (i.e., when the Ca^{2+} concentration in the ER is high) [18]. The EF-SAM domain oligomerizes upon a drop in the local Ca^{2+} concentration; oligomerization of the EF-SAM domain leads to structural rearrangements in its cytoplasmic regions [19], which, in turn, results in translocation toward the plasma membrane (PM), opening of the PM Ca^{2+} channel Orai1, and restoration of resting Ca^{2+} levels (Fig. 1B) [20]. STIM proteins thus play a central role in the regulation of Ca^{2+} release activated Ca^{2+} (CRAC) channel activation [21].

It has been shown *in vivo* that STIM1 activation is cooperative with respect to the luminal Ca^{2+} concentration [22,23], enabling STIM1 to robustly transduce chemical information into a quasi-binary mechanical signal across the ER membrane. Here, we demonstrate that the EF-SAM domain *by itself* exhibits cooperative dimerization and unfolding upon Ca^{2+} loss *in vitro* with a Hill coefficient and a half-maximal activation ($K_{1/2}$) that are very close to the values observed for STIM1 activation *in vivo*. The dissociation constant showed an exponential dependence on Ca^{2+} concentration, behavior often observed in chemically induced unfolding. Based on a wide range of *in vitro* experimental results, we propose a mathematical description of the EF-SAM/Ca^{2+} system that is both simple and distinct from current allosteric models.

The unfolding of the EF-SAM domain upon Ca^{2+} loss precluded structure determination of the apo form by NMR spectroscopy. However, by incorporating CD and analytical ultracentrifugation (AUC) results with *in silico* structural modeling, we were able to identify a putative dimer interface that was subsequently shown to be resistant to proteolytic cleavage. Taken together, this study places the STIM1 EF-SAM/Ca^{2+} system within a class of signaling proteins regulated by IDD-mediated cooperativity, which perhaps surprisingly leads us to a better understanding of its partially unfolded Ca^{2+}-free structure.

Results

The STIM1 EF-SAM domain forms soluble oligomers upon Ca^{2+} loss

It is known that the STIM1 EF-SAM domain forms oligomers upon Ca^{2+} depletion but remains monomeric when Ca^{2+} is abundant [17]. In order to further characterize this transition, we prepared EF-SAM domains at various Ca^{2+} concentrations in the range 0.0–1.0 mM and examined them by gel filtration. As Ca^{2+} concentrations were lowered, the peak elution volume shifted, consistent with the formation of oligomers (Fig. 2A). Two sharp peaks were formed at Ca^{2+} concentrations in ranges 0.0–0.1 and 0.5–1.0 mM, which were estimated to correspond to masses of approximately 70 and 27 kDa, respectively. If we associate the second peak with the known (17.4 kDa) monomeric state, then the first peak might correspond to that of a dimer. However, since protein unfolding can significantly affect elution time, we next examined the stoichiometry of the oligomerization reaction by other methods.

The EF-SAM domain forms predominantly dimers upon Ca^{2+} loss

To quantify the stoichiometry of EF-SAM oligomers as a function of Ca^{2+} concentration, we subjected the peak fractions from gel filtration to AUC analysis. Subsequent gel-filtration analysis (data not shown) confirmed that the protein solutions were stable over the time range of the AUC experiments. Consistent with the gel-filtration results, the effective molecular weights fitted to AUC measurements indicated that the STIM1 EF-SAM domain forms predominantly monomers and dimers but not higher-order oligomers, even at very low Ca^{2+} concentrations (Fig. 2B). Although some higher-order oligomers may form under some conditions, the AUC results indicate that, by far, the major oligomeric state is a dimer.

The dimerization reaction is cooperative with respect to Ca^{2+} concentration

Since the abovementioned initial analysis strongly indicates that the self-association of EF-SAM domain

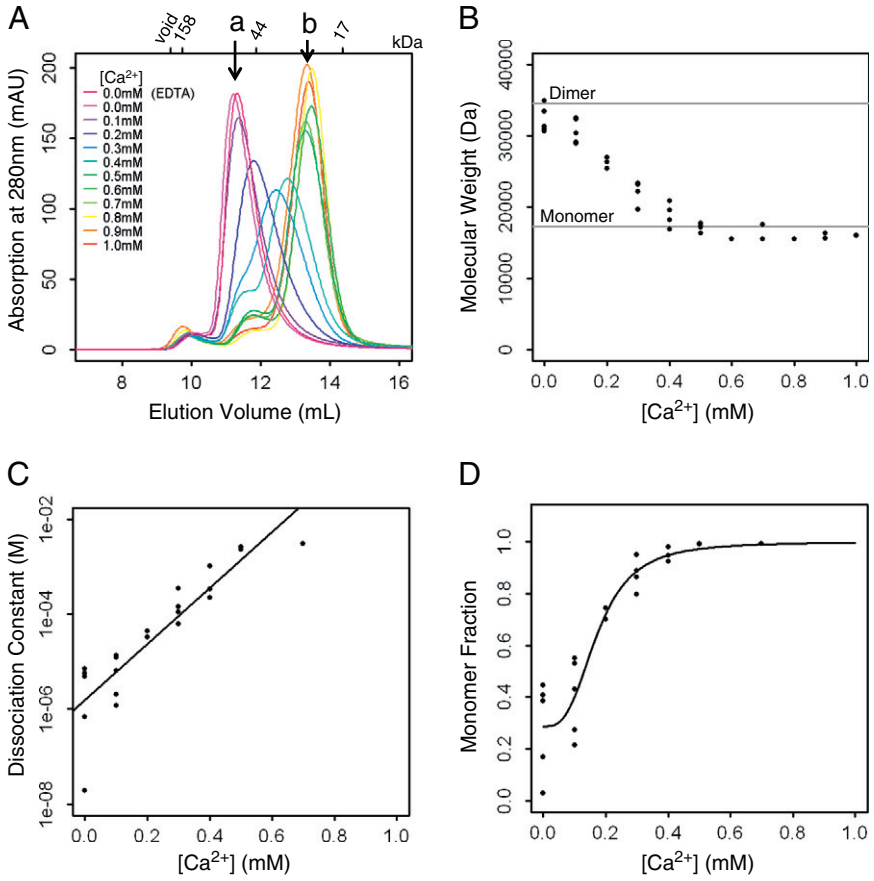

Fig. 2. Oligomeric state as a function of Ca^{2+}. (A) Peak elution volumes from analytical gel-filtration chromatography; the positions marked by arrows a and b correspond to estimated molecular masses of 70 and 27 kDa, respectively. (B) Effective molecular masses as determined by AUC. Each concentration of the protein is in the range 5.0 ~ 13.1 μM. (C) The effective equilibrium constant as given by AUC measurements. (D) Fractions of monomer as estimated from the effective equilibrium constants under the assumption of a fixed 10 μM protein concentration.

is dimeric, we calculated the dissociation constant for each sample by fitting the corresponding model to the AUC measurements [24]. The resulting dissociation constant showed an exponential dependence on Ca^{2+} concentration (Fig. 2C). The dissociation constants were then converted into monomer fractions of EF-SAM domain by assuming a fixed 10-μM protein concentration (Fig. 2D). We fit a Hill function with an offset to the monomer fractions [*m*]:

$$\frac{(1-a)\,[m]^n}{K_{1/2}^n + [m]^n} + a,$$

which gave a Hill coefficient of 3.0 ± 0.7 and a half-maximal activation ($K_{1/2}$) of 0.17 ± 0.02 mM. The use of the offset $a = 0.29 \pm 0.05$ reduced the AIC (*A*kaike *I*nformation *C*riterion) from −10.5 to −32.0 compared to a simple Hill function without offset. In addition, we confirmed that models without cooperativity ($n = 1$) have larger AIC values (−5.7 and −14.6; without and with an offset, respectively), which supports both our use of the model and the interpretation of the resulting Hill coefficient in terms of cooperativity. The Hill coefficient and $K_{1/2}$ are comparable to those observed *in vivo* for STIM1 redistribution (Hill coefficient = 3.8; $K_{1/2}$ = 0.19 mM) and CRAC current (Hill coefficient = 4.2; $K_{1/2}$ = 0.17 mM) [23]. Although it is natural to expect that many other phenomena (e.g., involvement of cytoplasmic domains, tethering to the membrane, etc.) contribute to the observed cooperativity *in vivo*, these results demonstrate that the EF-SAM domain alone is sufficient to exhibit cooperative oligomerization with respect to Ca^{2+} concentration. Below we explore the underlying physical mechanism for such cooperativity.

Cooperative oligomerization cannot be explained by a simple allosteric model

In order to assess whether a simple allosteric model can explain the observed cooperativity of the dimerization with respect to Ca^{2+} concentration, we

next modeled the reaction mathematically using conventional chemical reaction equations. Here, we assumed that all possible monomer and dimer forms of the EF-SAM domain could be accounted for by their Ca^{2+} binding states: [M'] and [M] represent the monomer concentrations with one and zero bound Ca^{2+} ions, respectively; [D''], [D'], and [D] represent the dimer concentrations with two, one, and zero bound Ca^{2+} ions, respectively. The possible reactions among these molecular species are as follows: $M + Ca^{2+} \leftrightarrow M'$, $D + Ca^{2+} \leftrightarrow D'$, $D' + Ca^{2+} \leftrightarrow D''$, $D \leftrightarrow 2M$, $D' \leftrightarrow M + M'$, $D'' \leftrightarrow 2M'$, $D + Ca^{2+} \leftrightarrow M + M'$, and $D' + Ca^{2+} \leftrightarrow 2M'$, which results in eight equilibrium constants. Note that the reactions above are general enough to incorporate potential allostery via cooperativity mediated by the two cEF-hands of the dimer; that is, the association constant for a dimer with one bound Ca^{2+} (D') and a free Ca^{2+} ion can be different from that for a dimer without a bound Ca^{2+} (D) or for an unbound monomer (M). For simplicity, in the following analysis, we assumed that the Ca^{2+} concentration was much higher than that of the protein and thus ignored changes in Ca^{2+} concentration due to protein binding. Also, because we were interested in the equilibrium *in vitro* without inflow of energy, we further assumed a condition of *detailed balance*, which relates equilibrium constants to each other. The system is then described by three association constants for Ca^{2+},

$$K_a = \frac{[M']}{[M]\left[Ca^{2+}\right]}$$

$$K_a' = \frac{[D']}{[D]\left[Ca^{2+}\right]}$$

$$K_a'' = \frac{[D'']}{[D']\left[Ca^{2+}\right]},$$

and one dissociation constant for the dimer without Ca^{2+} binding,

$$K_d = \frac{[M]^2}{[D]}.$$

The final expression for the effective dissociation constant of the EF-SAM domain can then be written as:

$$K_d^{eff} \equiv \frac{([M] + [M'])^2}{[D] + [D'] + [D'']} = \frac{\left(1 + K_a\left[Ca^{2+}\right]\right)^2 K_d}{1 + K_a'\left[Ca^{2+}\right] + K_a' K_a''\left[Ca^{2+}\right]^2}.$$

From the resulting expression, it can be seen that the monomer concentration ([M] + [M']) is at most linear with respect to Ca^{2+} concentration, and thus, this system does *not* show cooperativity in monomer fraction with respect to Ca^{2+} concentration as in Fig. 2D. One might have imagined a scenario in which the dimer binds two Ca^{2+} ions in a cooperative manner; however, the subsequent dissociation into two monomers, each of which contains a single Ca^{2+}-binding site, cancels out this nonlinear dependence on Ca^{2+} in the abovementioned system of equations. The abovementioned formulation is general given three basic assumptions: (1) that the Ca^{2+} concentration is much greater than the protein concentration; (2) the condition of detailed balance; and (3) that there are only two monomer and three dimer protein species to be considered. Since the resulting effective dissociation constant does not agree with the exponential Ca^{2+} concentration dependence obtained by our AUC measurements (Fig. 2C), we must reject one or more of these assumptions. The first is justified: Ca^{2+} concentrations were indeed much higher than protein concentrations except for in the completely Ca^{2+} free samples. The second assumption is more of a convenience that allows us to write the equations in a compact form; relaxing the detailed balance condition does not result in the appearance cooperatively. However, the third assumption—that the protein states can be described simply by the occupancy of their Ca^{2+}-binding sites—is not justified, since Ca^{2+} concentration is known to affect the stability of the EF-SAM domain, as discussed in detail below. This forces us to conclude that it is impossible to treat the dimeric EF-SAM domain as a simple allosteric system.

As mentioned in Introduction, Hilser and Thompson predicted that IDDs could facilitate allosteric coupling [9], and these predictions have been borne out in recent experiments [5–8]. Thus, it is worth investigating whether the lack of cooperativity in monomer fraction with respect to Ca^{2+} concentration in our chemical reaction equations above can be resolved using their framework for modeling IDDs. For this purpose, we introduced additional unfolded states and possible allosteric changes of the free energy depending on conformation, following the Hilser–Thompson formulation. However, even when these unfolded species are explicitly included, the description of the cooperativity in monomer fraction with respect to [Ca^{2+}] does not qualitatively change (see Appendix A). Thus, in spite of the apparent similarity to the system considered by Hilser and Thompson, we conclude that the mechanism of STIM1 EF-SAM dimerization upon unfolding is distinct from their mechanism. It has been suggested that the hEF-hand motif contributes to the *in vivo* cooperativity of STIM1 [20]; however, since only the cEF-hand motif has actually been shown to bind Ca^{2+}, it is not clear how the presence of the hEF-hand motif would give rise to cooperative dimerization. These questions further

motivated us to analyze the structural diversity of EF-SAM domain as a function of Ca^{2+} concentration.

The EF-SAM domain cooperatively unfolds in response to Ca^{2+} depletion

It has been shown that, upon Ca^{2+} loss, the helical content of the STIM1 EF-SAM domain decreases dramatically [17]. To understand the transition in more detail, we examined the secondary structure of EF-SAM domain at various Ca^{2+} concentrations in the 0.0- to 1.0-mM range using CD spectroscopy. The CD spectra of the STIM1 EF-SAM domain at 0.0 and 1.0 mM [Ca^{2+}] agreed well with those reported previously [17], and at intermediate Ca^{2+} concentrations, the spectra fell between these two extremes (Fig. 3A). The change in CD ellipticity at 222 nm obeyed a sigmoidal dependence on [Ca^{2+}] (Hill coefficient = 4.7 ± 0.6; $K_{1/2}$ = 0.26 ± 0.01 mM), similar to that observed in AUC measurements of the monomer/dimer transition (Fig. 3B). The CD spectra indicated that the alpha helical content dropped upon Ca^{2+} depletion from a value of >50% to nearly 10%; over the same range of Ca^{2+} concentration values, the beta strand content remained low (~10%) (Fig. 3C). The CD spectra are consistent with the known helix-rich structure of the EF-SAM domain under Ca^{2+}-loaded conditions and partial unfolding upon Ca^{2+} loss [16]. A fit to the alpha helical content returned a Hill coefficient = 5.9 ± 0.6 and $K_{1/2}$ = 0.25 ± 0.01 mM, which is qualitatively similar to the result based on the change in ellipticity. In summary, upon Ca^{2+} loss, the STIM1 EF-SAM domain undergoes a cooperative transition from a well-folded state to a mostly unstructured state that mirrors the *in vitro* dimerization reaction and the *in vivo* STIM1 redistribution and CRAC current processes. These results strongly suggest that protein unfolding may be involved in the cooperativity observed in the dimerization reaction.

NMR analysis indicates EF-SAM dimers in dynamic equilibrium

We next examined the NMR spectra of the EF-SAM domain at Ca^{2+} concentrations spanning the critical Ca^{2+} concentration for the monomer/dimerization transition. The two-dimensional ^{1}H-^{15}N heteronuclear single-quantum correlation (HSQC) spectrum of the STIM1 EF-SAM domain at 0.5 mM [Ca^{2+}] (Fig. 4A) agreed well with published spectra [17]. The ^{1}H and ^{15}N chemical shifts were well dispersed, and each peak was sharp, suggesting that the protein was stably folded and existed in a monomeric state. As the Ca^{2+} concentration was reduced, the positions of well-dispersed peaks did not shift significantly; rather, they displayed a gradual loss in peak intensity accompanied by an accumulation of intensity in the poorly dispersed (i.e., central) part of the spectrum, characteristic of dynamic exchange between oligomers, conformational flexibility, or both (Fig. 4B and C). At 0.1 mM [Ca^{2+}], the spectrum resembled the previously reported Ca^{2+}-depleted state [17] (Fig. 4D). Although gel-filtration and AUC measurements indicated that, *in vitro*, soluble EF-SAM oligomers consist almost entirely of dimers in the absence of Ca^{2+}, the NMR spectra strongly suggested that partially unfolded EF-SAM dimers are not static and may consist of an ensemble of conformational states, consistent with the CD results. Since we could not observe the apo EF-SAM domain structure experimentally, we next examined the dynamics of the structure computationally.

MD and sequence analysis indicate additional intermediate states and intrinsic disorder of EF-hands upon Ca^{2+} loss

Based on the abovementioned observations, a qualitative interpretation of the observed dimerization dependence on Ca^{2+} is that Ca^{2+} binding

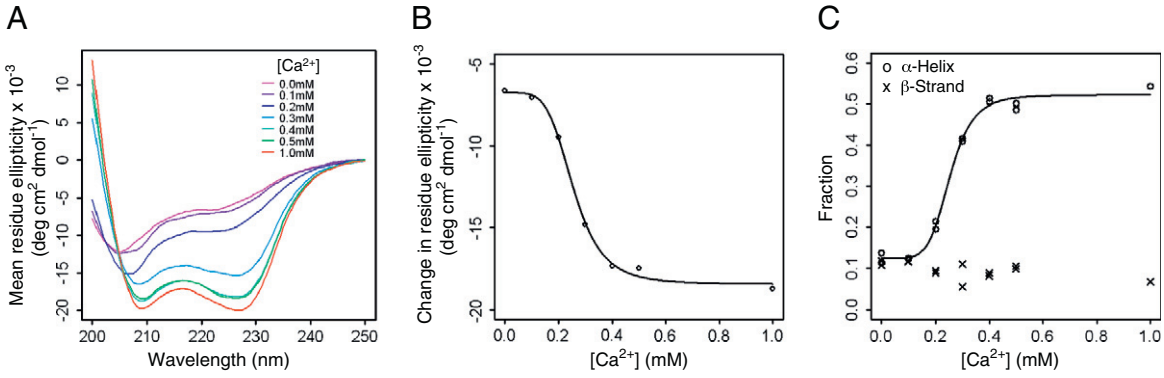

Fig. 3. Structural changes as a function of [Ca^{2+}]. (A) CD spectra of EF-SAM domain at various Ca^{2+} concentrations. (B) Ellipticity at 222 nm. (C) Secondary structure content estimated from all CD measurements, where circles represent the estimated alpha helical fraction and crosses represent beta strand fraction. The lines represent curves fitted using a Hill equation with offset.

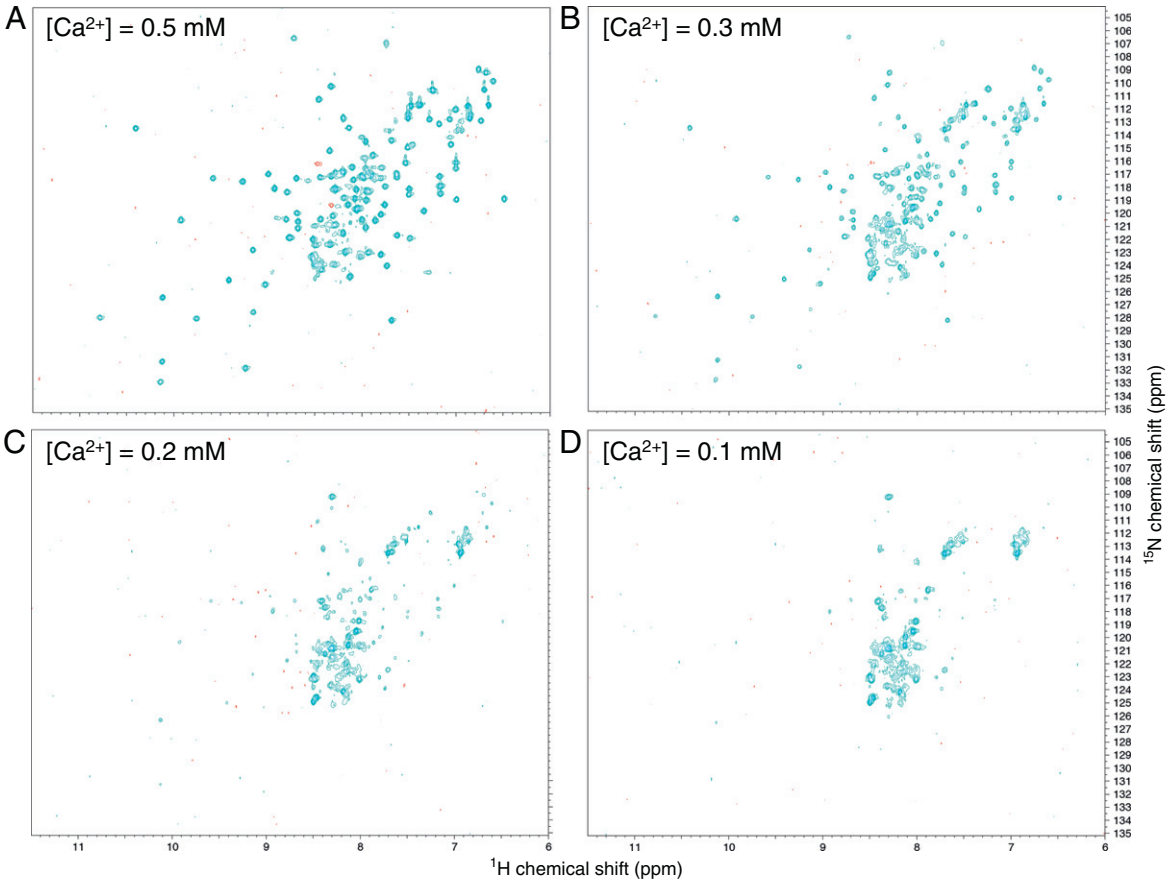

Fig. 4. ^{1}H-^{15}N HSQC spectra. NMR spectra were acquired at four Ca^{2+} concentrations, as indicated. Red peaks are of the resonances of $^{1}H^{\varepsilon}$-$^{15}N^{\varepsilon}$, which appear at aliased positions.

requires a well-folded protein, which, in turn, requires high Ca^{2+} concentrations. Conversely, dimerization of the EF-SAM domain is likely to occur by interaction between exposed hydrophobic residues [16], which occurs only when Ca^{2+} concentrations are low enough to promote unfolding. In order to better understand the structural response of the EF-SAM domain to Ca^{2+} loss, we carried out replica exchange simulations of the Ca^{2+}-bound and Ca^{2+}-free STIM1 EF-SAM domain. A heat capacity–temperature diagram was used to find the transitions (Fig. 5A) from which energy histograms and intermediate representative conformations were identified (Fig. 5B). To compare the stability of the apo and holo EF-SAM monomers, we calculated their specific heats (C_V) at different temperatures by applying the weighted histogram analysis method [25]. The sharp peaks in the C_V–T diagram indicate unfolding transition events. The temperature of the first transition of the apo EF-SAM domain was at approximately 295 K, which was reported as 21 °C based on CD thermal unfolding experiments [26]. The corresponding temperature in the holo form shifted to 314 K. Interestingly, we observed an intermediate state, which features a shoulder at 322 K in the apo form that is not observed in the holo unfolding simulations (Fig. 5C). The existence of an additional intermediate state may be one reason why the apo form unfolds more easily compared to the holo EF-SAM domain. The apo molecular dynamics (MD) trajectory in explicit water indicated that electrostatic repulsion between negatively charged residues in the EF-hands promoted unfolding under conditions of reduced Ca^{2+} concentration. The EF-hands are predicted to become intrinsically disordered in the absence of Ca^{2+}, as indicated by both the RMSF (*r*oot-*m*ean-*s*quare *f*luctuation) computed from the explicit water MD simulation and sequence-based intrinsic disorder prediction [27] (Fig. 5D), consistent with both CD and NMR measurements. From these simulations, we can see that the hEF-hand, while not explicitly involved in binding Ca^{2+}, contributes significantly to the instability of the EF-SAM domain.

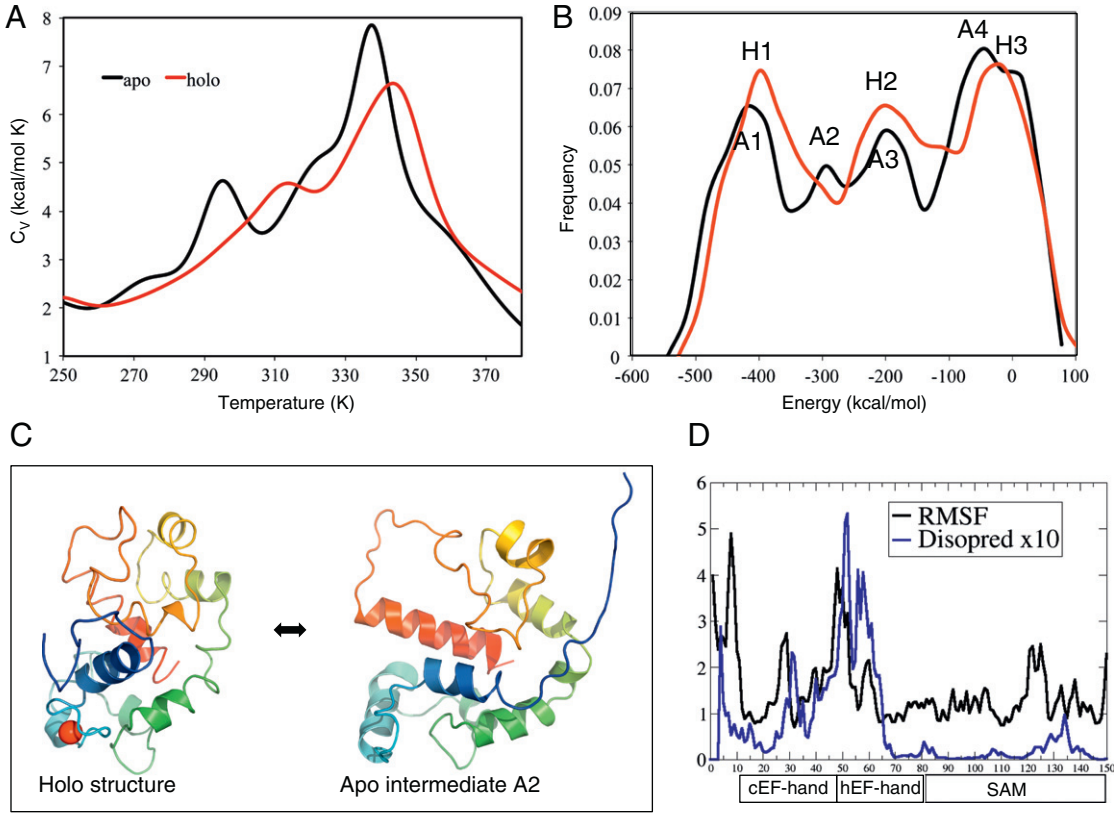

Fig. 5. EF-SAM unfolding. (A) The specific heat is plotted as a function of temperature for apo and holo trajectories. (B) Energy histograms indicate stable transition states A1-4 and H1-3 for apo and holo simulations, respectively. (C) The intermediate state A2 observed in the apo but not in the holo simulation. (D) RMSF (black line) and intrinsic disorder (blue line) are shown as a function of residue number.

Ca^{2+} loss effectively acts as a chemical denaturant for the EF-SAM domain

As described above, simple allosteric models assuming a finite number of distinguishable protein states do not explain the observed exponential Ca^{2+} concentration dependence of the dissociation constant (Fig. 2C). Since CD and NMR measurements and MD and sequence-based calculations all indicate that reduction of Ca^{2+} leads to an increase in the diversity of conformational states, an alternate approach is to introduce continuous changes in protein stability depending on the Ca^{2+} concentration through a thermodynamics-based description of the system. We modeled the EF-SAM domain as an equilibrium between monomeric and dimeric states at a given Ca^{2+} concentration, $2\mu \leftrightarrow \delta$, where μ and δ include all possible conformations of monomers and dimers, respectively, including both Ca^{2+}-free and Ca^{2+}-bound forms. The equilibrium should then be specified by the difference in the free energy as:

$$K_d \propto e^{\frac{-\Delta G\left(\left[Ca^{2+}\right]\right)}{RT}},$$

where R is the gas constant and T is the temperature. Here, we have assumed that the difference in the free energy, $\Delta G([Ca^{2+}])$, between the monomeric and dimeric states, is Ca^{2+} concentration dependent. That is, the landscape of the free energy with respect to Ca^{2+} concentration is contained in the functional form of $\Delta G([Ca^{2+}])$. Although the exact functional form is not known, we can nevertheless expand K_d to first order for small changes in Ca^{2+} concentration, which gives

$$K_d \propto e^{\frac{-\left[Ca^{2+}\right]\Delta G'}{RT}},$$

where $\Delta G'$ is the derivative of the free energy with respect to the Ca^{2+} concentration. This result implies that the effective equilibrium constant should, over small ranges, follow an exponential dependence on Ca^{2+} concentration. Although highly simplified, the abovementioned derivation agrees remarkably well with the AUC data for Ca^{2+} concentrations in the range 0.0–0.7 mM (Fig. 2C). In addition, from the fitted line, we could estimate that $\Delta G'$ is -7.5 ± 0.8 kcal mol^{-1} mM^{-1}. We then

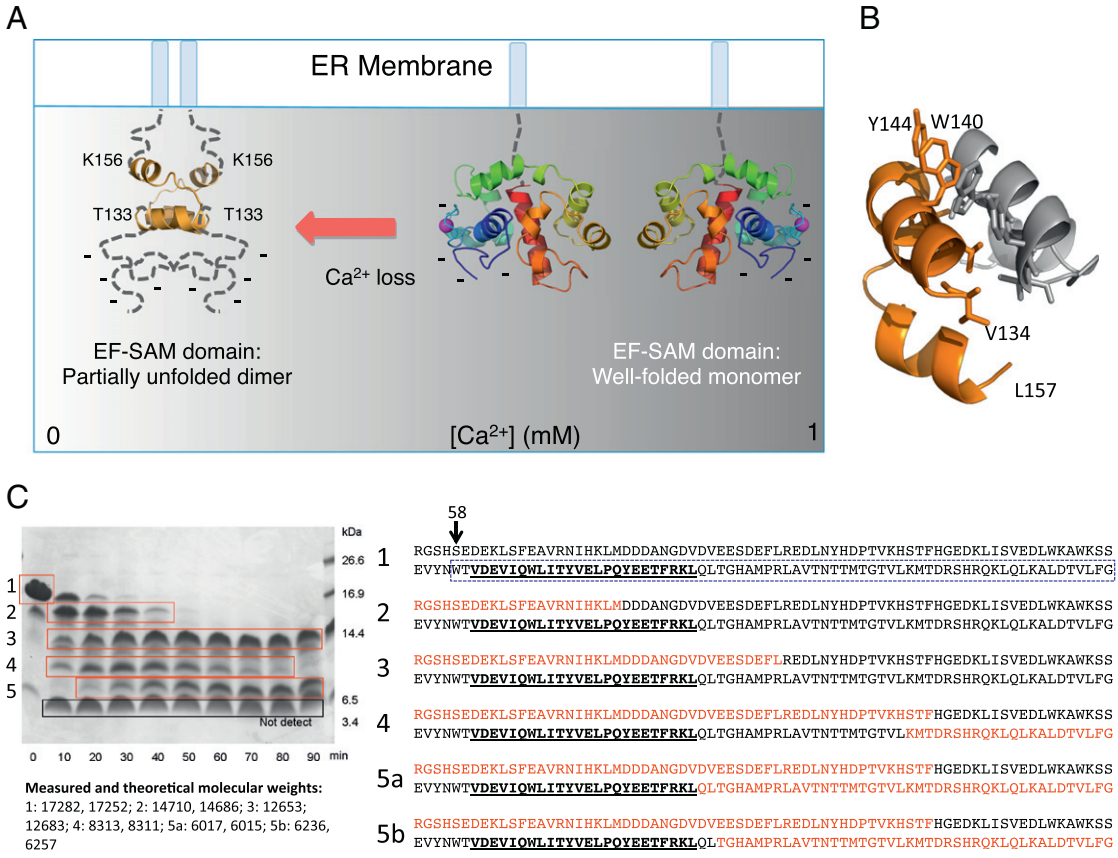

Fig. 6. Proposed model of EF-SAM dimerization. (A) The right side of the figure shows the Ca^{2+}-bound EF-hand monomers at high Ca^{2+} concentration with negative charges concentrated near the well-folded EF-hands. The left side of the figure shows the partially unfolded dimer with negative charges of the disordered EF-hands distributed over a wider volume of space and the stable SAM N-terminal helical hairpins forming the intermolecular dimer interface. (B) Rigidly self-docked homodimer model of segment V134–L157 extracted from the calcium-bound EF-SAM domain with hydrophobic and aromatic residues shown in stick representation. (C) Proteolysis experiments. The left panel shows the time course of proteolysis by chymotrypsin, and the right panel shows the sequence segments with digested residues in red and the predicted dimer interface indicated by underlined boldfaced characters. The boundary of the SAM domain is indicated by a blue dotted box in segment 1. There was a two-residue ambiguity in the fifth segment, as indicated in 5a and 5b. Note: the full-length EF-SAM sequence includes a four-residue extension (PLCH) carried over from the plasmid used for overexpression.

estimated change in free-energy difference with respect to the monomer between 0.0 and 0.5 mM $[Ca^{2+}]$ at 4 °C by $|0.5\ mM \times \Delta G'|/2 = 1.9 \pm 0.2$ kcal mol^{-1}. This value is of the same order as the experimentally measured value (3.2 kcal mol^{-1}) at 10 °C [17].

The exponential dependence of the effective equilibrium constant with respect to the decrease in Ca^{2+} concentration is analogous to that often observed in unfolding by chemical denaturation, in which the free energy shows a linear dependence on denaturant concentration [28,29]. Taken together, these results strongly indicate that Ca^{2+}-dependent protein unfolding drives the cooperative dimerization of STIM1 EF-SAM domain.

Proposed model of STIM1 EF-SAM dimerization

The observations above enable us to propose a structural model for the Ca^{2+}-dependent unfolding/dimerization reaction (Fig. 6A). The CD results indicate that the apo form of the STIM1 EF-SAM has a helical content of only 12–13%, corresponding to ~19 residues or ~5 full helical turns. It is likely that these remaining helical residues form at least part of the dimer interface, since regular secondary structures are much more predominant than loops at homodimeric interfaces [30]. Furthermore, the fact that only dimers and not higher-order oligomers are observed in solution suggests that the dimers form a closed (i.e., head-to-head) structure. Finally, according to both

sequence-based analysis and MD simulations, the most stable regions in the EF-SAM domain consist of helices located in the SAM domain. The above-mentioned observations imply that EF-SAM dimerization is likely to occur through interaction of approximately 5 helical turns in the SAM domain. There are two candidate regions that contain the appropriate number of helical turns in the SAM domain that are stable upon unfolding simulations: the SAM C-terminal helix (D183–F200) and the SAM N-terminal helical hairpin (V134–L157). To assess the relative likelihood of the SAM C-terminal helix or the SAM N-terminal helical hairpin to homodimerize, we extracted each from the native Ca^{2+}-bound structure and self-docked. High-scoring docked homodimers were then subjected to explicit water MD simulations. Asymmetric dimer structures were excluded in consideration of the transmembrane helix that would constrain dimerization *in vivo*; however, we cannot rule out the possibility that asymmetric dimers might form. The dimer composed of two SAM C-terminal helices was found to be highly unstable due to electrostatic repulsion between positively charged residues (R184, R187, K189, K193). In contrast, the SAM N-terminal helical hairpin was stabilized through pairing of a hydrophobic face (V134, V137, L141, V145) and stacking between aromatic groups W140 and Y144 (Fig. 6B). The proposed dimer interface of the SAM N-terminal helical hairpin model was subsequently shown to be resistant to proteolysis by chymotrypsin (Fig. 6C). In fact, the proteolysis results show very close agreement with the sequence-based intrinsic disorder prediction and the MD-based RMSF calculation (Fig. 5D), which both indicate that, in addition to the SAM domain, a small C-terminal portion of the hEF-hand is stable.

The EF-hands are rich in Asp/Glu compared with Arg/Lys (21 *versus* 8 residues, respectively). At high Ca^{2+} concentrations, the folded EF-SAM domain buries hydrophobic groups and concentrates negatively charged residues at the surface of a compact globular domain. This high surface charge density is likely to prevent EF-SAM dimerization under Ca^{2+}-loaded conditions. Upon Ca^{2+} depletion, the EF-hand domains become disordered and distribute their charges over a larger volume of space. Dimerization via pairing of exposed hydrophobic residues in the SAM N-terminal helices can then proceed.

Discussion

Recently, a number of reports have demonstrated the important role of conditional disorder in signaling molecules [4]. Since, by definition, disordered regions in proteins are difficult to observe, it is likely that their importance has been underappreciated compared to the role of ordered domains. Similarly, the role of disorder-mediated cooperativity has only recently been experimentally studied [5–8]. The cooperative oligomerization of STIM1 is important for its role in responding to Ca^{2+} depletion within the ER. It has previously been shown that oligomerization of the STIM1 luminal region is necessary for translocation to the ER–PM junction and subsequent opening of the Orai1 channel [23]. However, the direct relationship between STIM1 oligomerization and Ca^{2+} binding has not been described. Our *in vitro* measurements indicate that the dominant oligomerization reaction of the EF-SAM domain is that of monomer/dimer equilibration and that the dimerization is cooperative with respect to Ca^{2+} concentration. Interestingly, the Hill coefficient and $K_{1/2}$ of the *in vitro* reaction are very close to the *in vivo* values for STIM1 redistribution and CRAC current intensity as a function of ER Ca^{2+} concentration [23].

In order to deepen our understanding of the underlying mechanism of this cooperativity, we investigated the conformational changes in the EF-SAM domain that occur upon Ca^{2+} depletion. The CD and NMR spectra presented here agreed with previous reports [17] and indicated that loss of defined structure and dimerization occur concurrently; the NMR results also strongly suggested that EF-SAM oligomers exist in dynamic equilibrium. MD simulations and sequence analysis were consistent with these observations and indicated that the order-to-disorder transition is driven by unfolding of the EF-hand motifs. We observed an additional intermediate state in the apo MD simulation that was not present in the holo simulation that may be important for rapid unfolding.

In order to quantify the dependence on Ca^{2+} concentration without having to treat each microscopic conformational state explicitly, we expanded the free energy to first order and obtained an exponential dependence of the monomer/dimer equilibrium constant on Ca^{2+} concentration. This relationship is far more sensitive than what would be obtained from treating the single Ca^{2+}-binding site explicitly with classical chemical reaction equations and agrees remarkably well with the AUC results over a wide range of Ca^{2+} concentrations. Interestingly, this result implies that, to first order, the free energy depends linearly on Ca^{2+} concentration, a result commonly observed in equilibrium unfolding by chemical denaturation [28,29]. This interpretation suggests that although the hEF-hand domain is not a classical allosteric site, or even a Ca^{2+}-binding site, it is highly prone to disorder and thus plays an important role in coordinating EF-SAM responses to Ca^{2+} loss.

It has recently been shown that dimerization of the STIM1 luminal region results in conformational changes in the cytoplasmic region that lead to Orai1 channel opening [19]. In this same study, the authors argue that, since a STIM1 dimer contains only two

Ca^{2+}-binding sites, the observed cooperativity of Orai1 activation *in vivo* requires high-order oligomerization [19]. Here, we present an alternative view in which EF-SAM dimerization is itself cooperative with respect to Ca^{2+} concentration owing to intrinsic disorder rather than higher-order effects. If we accept that the dimerization of the EF-SAM domain is cooperative, it is reasonable to assume that all downstream events, including CRAC channel opening, will be cooperative as well. This is not to say that cytoplasmic PPIs or higher-order oligomerization do not contribute quantitatively to the observed cooperativity *in vivo*. Rather, what the results presented here imply is that the EF-SAM dimerization reaction is itself sufficient for mediating cooperativity to a degree that is observed *in vivo*. In this respect, it is worth noting that the Hill coefficients measured in two different *in vivo* studies of STIM1 activation [22,23] differed by approximately a factor of 2.

The functional importance of the order-to-disorder transition in STIM1 has been discussed previously [16]. Since protein folding in general [31] and folding of multiple EF-hand domains in particular [32] has been shown to be a cooperative process, and since dimerization of STIM1 depends on unfolding, it is perhaps not surprising that STIM1 exhibits cooperative dimerization. Nevertheless, to our knowledge, even a qualitative model of STIM1 cooperativity based on Ca^{2+} dependent unfolding of the EF-SAM domain has not been proposed previously. Here, we present a mathematical model that both agrees with experimental observations and describes the cooperativity quantitatively. From a biological point of view, this model is interesting because it implies that the stability of the EF-hands precisely and robustly determines the Ca^{2+} concentration threshold for EF-SAM dimerization.

We further show that the exponential dependence of the dimerization dissociation constant on Ca^{2+} concentration does not follow from modeling by either chemical reaction equations or the Hilser–Thompson model of IDD-mediated allostery. The STIM1 EF-SAM/Ca^{2+} system is clearly allosteric in the conventional sense that Ca^{2+} binding drastically influences the EF-SAM homodimerization dissociation constant. However, since, strictly speaking, all dynamic proteins are allosteric [33], and since current allostery models do not capture the Ca^{2+} concentration dependence, the label "allosteric" would seem to be insufficient to describe the STIM1 EF-SAM/Ca^{2+} system. Moreover, this may not be an isolated case, given the abundance of EF-hand domains in signaling proteins [34].

Our interpretation of the cooperativity mechanism is consistent with the observation that the homologous protein STIM2, which is more stable than STIM1 [35], exhibits lower cooperativity with respect to Ca^{2+} concentration [22]. This, in turn, implies that protein stability might tune the kinetics and thermodynamics of other important PPI networks, an intriguing prospect given the abundance of disorder-containing proteins in eukaryotes.

The *in vitro* experiments and simulations discussed here allowed us to propose a structural model of the Ca^{2+}-dependent dimerization reaction (Fig. 6). In this model, dimerization is predicted to occur via pairing of exposed hydrophobic residues in the SAM domain. We identified two potential dimerization interfaces, one that involves the SAM C-terminal helix and the other involving the SAM N-terminal hairpin. Our flexible docking simulations indicated that the SAM N-terminal hairpin dimer is much more likely to form due to packing of hydrophobic residues and stacking of aromatic residues; in contrast, strong electrostatic repulsions in the hypothetical SAM C-terminal dimer render this model infeasible. This SAM N-terminal hairpin dimer model is admittedly speculative but is supported by experiments showing that the predicted dimer interface corresponds exactly to the portion of the SAM domain that is protected upon proteolysis. The dimer model suggests a novel route for controlling STIM1 activation by dimer inhibition, which is important for activation in immune cells. Although STIM1 and Orai1 are broadly expressed in mammalian tissues, the clinical phenotype of severe combined immunodeficiency patients is predominantly that of immunodeficiency. Given that the inhibition of SOCE by attenuation of STIM1 or Orai1 function results in amelioration of allergy [11], autoimmunity [36], and inflammation [37] in animal models, artificial inhibition of the partially unfolded EF-SAM dimer may open new avenues to the development of beneficial therapies.

Materials and Methods

Purification of EF-SAM fragment

A His-tagged EF-SAM fragment from STIM1 in mouse was overproduced in *E. coli* Rosetta2 (DE3) pLysS carrying pET28a. Cells were grown in L broth medium containing 30 mg l^{-1} chloramphenicol and 20 mg l^{-1} kanamycin at 37 °C. When the optical density at 600 nm reached 0.5–0.6, isopropyl-beta-D-thiogalactopyranoside was added to a final concentration of 1 mM for induction of the expression. After additional 27 h growth, cells were harvested by centrifugation at 7000*g* for 10 min. The cells were suspended in buffer A (10 mM Tris–HCl at pH 8.0) with a tablet of protease inhibitor cocktail (Boehringer Mannheim). The cell suspension was sonicated (AsTRASON model XL2020 sonicator; Misonix Inc.) on ice and centrifuged at 80,000*g* for 20 min. His-EF-SAM was found in the precipitant. After suspending the precipitant in buffer B (buffer A supplemented with 100 mM NaCl) containing 1% Triton X-100, we sonicated and centrifuged the suspensions. The precipitant was then suspended in buffer B containing 2% beta-octylglucoside and centrifuged. The precipitant was further suspended in buffer B containing 6.0 M urea and centrifuged. The supernatant was loaded onto a Q-Sepharose FF column

(5 ml) (GE Healthcare) equilibrated and washed with buffer A containing 6.0 M urea. After the elution of unbound species, His-EF-SAM was eluted with an NaCl gradient of 50%/10 cv. The solution diluted twice with buffer A was loaded onto a Q-Sepharose HP column (5 ml) (GE Healthcare), equilibrated, and washed with buffer A containing 6.0 M urea. After the elution of unbound species, His-EF-SAM was eluted with an NaCl gradient of 50%/5 cv. Then, the sample fraction was loaded onto a gel-filtration column, Superose 12 HR 10/30 column (GE Healthcare), equilibrated with buffer A containing 150 mM NaCl and 6.0 M urea. For concentration of the protein-containing fraction, the sample was loaded onto a Q-Sepharose HP column (5 ml) and eluted with an NaCl gradient of 50%/5 cv. The fraction containing His-EF-SAM was concentrated with buffer C (buffer B supplemented with 5 mM $CaCl_2$) containing 20% polyethylene glycol 20,000. The His-tag was removed using proteolytic cleavage by adding thrombin (GE Healthcare). The reaction was carried out at room temperature for 100 min in buffer C at thrombin and protein concentrations of 25 units ml^{-1} and 0.5 mg ml^{-1}, respectively. To remove the N-terminally His-tagged peptide, non-cleaved His-EF-SAM, and thrombin, we loaded the sample solution onto a gel-filtration column, Superdex 75 10/30 column (GE Healthcare), and equilibrated it with buffer C.

Analytical ultracentrifugation

Sedimentation equilibrium AUC was performed using a Beckman Optima XL-A analytical ultracentrifuge with an An60Ti rotor (Beckman Coulter). The proteins were dissolved in buffer B containing various concentrations of $CaCl_2$ (0.0–1.0 mM). Measurements were conducted at 4 °C at three different speeds using charcoal-filled Epon centerpieces and Quartz windows. Concentration profiles of the protein samples were monitored by absorbance at a wavelength of 280 nm and recorded at a spacing of 0.001 cm in the step mode, with 20 averages per step, for 10, 14, and 18 h after each rotor speed was reached. Equilibrium data were analyzed using Beckman OptimaTM XL-A/XL-I data analysis software, version 6.04, provided as an add-on to Origin version 6.0 (MicroCal Inc.). The partial specific volume of EF-SAM at 4 °C, 0.721 ml g^{-1}, was estimated based on the amino acid composition of each protein.

Analytical gel-filtration chromatography

Analytical gel-filtration chromatography of EF-SAM containing several $CaCl_2$ concentrations was performed with Superdex 75 HR 10/30 column (GE Healthcare) with a path length of 0.5 cm. Gamma-globulin (158 kDa), ovalbumin (44 kDa), myoglobin (17 kDa), and vitamin B12 (1.4 kDa, data not shown) were used as size markers.

Circular dichroism

Far-UV CD spectra (200–250 nm) were measured on a Jasco-720 spectropolarimeter with a Peltier type cell holder, which allows for temperature control (JASCO International Co., Tokyo, Japan). Cylindrical fused quartz cells with 1 mm path length were filled with 0.06 mg ml^{-1} protein dissolved in buffer B and various concentrations of $CaCl_2$. Spectra were obtained by averaging five successive accumulations with a wavelength step of 0.5 nm at a rate of 20 nm min^{-1}, a response time of 8 s, and a bandwidth of 2.0 nm. The CD spectra were analyzed with the K2D2 program for prediction of secondary structure [38].

NMR spectroscopy

EF-SAM labeled uniformly with a ^{15}N stable isotope was expressed by culturing the transformed bacteria in an M9 minimal medium containing 1.0 g l^{-1} $^{15}NH_4Cl$ as the sole nitrogen source. The protein was purified as described above and prepared at a protein concentration between 11.0 and 12.2 μM dissolved in buffer B containing 10% (v/v) D_2O for the NMR lock. NMR spectra were acquired at 293 K with a Bruker Avance III 950 spectrometer equipped with a triple resonance (^1H, ^{15}N, and ^{13}C) cryogenic TCI probe with a *z*-axis gradient coil. For the two-dimensional ^1H-^{15}N HSQC spectroscopy experiments, the ^1H carrier was set at the frequency of the water resonance (4.821 ppm), and the ^{15}N carrier, at 119.63 ppm. The spectral widths (sampling complex numbers) were set at 2994 Hz (150*) and 18,939 Hz (1536*) for the ^{15}N and ^1H dimensions, respectively. For each free-induction decay, 128 scans were accumulated. Measurement of each spectrum took 22 h.

Proteolysis

The calcium-free EF-SAM domain was subjected to digestion by chymotrypsin in buffer B at 25 °C. Chymotrypsin was added to an EF-SAM domain solution at a protein concentration of 1.0 mg ml^{-1}, at a ratio of chymotrypsin to EF-SAM domain of 1:500 (w/w). Samples were collected every 10 min, followed by SDS-PAGE analysis to observe the state of digestion. We then analyzed the samples by mass spectrometry acquired with an Autoflex TOF instrument (Bruker Daltonics) to identify the amino acid sequence of proteolytic products.

Biochemical reaction equations

Canonical biochemical reaction equations with mass action were used to model the EF-SAM dimerization. In this analysis, the change in the Ca^{2+} concentration due to binding to the EF-SAM domain was ignored since the Ca^{2+} concentration was much higher than the EF-SAM concentration in the range of interest.

Molecular dynamics

Discrete molecular dynamics (DMD) simulations [39,40] were carried out using the holo SAM-EF domain structure (Protein Data Bank identifier 2k60) [16] as a starting conformation. For apo SAM-EF, the Ca^{2+} atom was removed from the structure. Both apo and holo structures were optimized by minimizing clashes using short all-atom DMD simulations at high temperature (~350 K). To compare unfolding transitions of apo and holo EF-SAM domains, we performed 50-ns replica exchange DMD simulations [41,42] using 18 replicas with temperatures ranging from ~240 K to ~380 K. The weighted histogram analysis method [25] was used to calculate specific heats (C_v) at different

temperatures. Representative intermediate states were selected by extracting conformations ±2 kcal mol^{-1} from each peak in the energy histogram, clustering with respect to pairwise root-mean-square deviation and retaining the centroid conformation of each cluster. RMSF calculations were based on an 80-ns MD simulation in explicit water using the cosgene/myPresto package [43] with AMBER potential and TIP3P water model.

Flexible docking

The surFit server‡ was used to generate rigidly docked initial structures, which were then refined by explicit water MD simulations, as described above.

Acknowledgments

The authors would like to thank Ms. Yuriko Suenari for her useful advice and Ms. Aya Takamori for help with mass spectrometry measurements. This work was supported by a combined research grant, provided by IFReC to D.M.S. and Y.B., by the Platform for Drug Discovery, Informatics and Structural Life Science, and by the Grant-in-Aid for Scientific Research on Innovative Areas "Harmonized Supramolecular Motility Machinery and Its Diversity" (No. 25117501) to Ms. Aya Takamori.

Appendix A. Inclusion of distinguishable unfolded states

In the text, we show that a simple model based on chemical reaction equations does not recapitulate the observed cooperative Ca^{2+} dependence of the monomer fraction (Fig. 2D). We then remarked that even when additional unfolded states are considered, as in the Hilser–Thompson framework, the cooperativity in the monomer fraction does not appear. In this appendix, we will clarify this point by including distinguishable unfolded state a la Hilser–Thompson in our system.

First, let us review the original Hilser–Thompson framework briefly. In their work, the authors considered a protein with two binding sites, I and II with the corresponding ligands A and B. They assumed that these binding sites can take both folded and unfolded forms whose free-energy differences are ΔG_{I} and ΔG_{II}. In addition they introduced an interaction energy Δg_{int} between the folded binding sites. Then, in equilibrium without ligand A, the probability of having a folded binding site for ligand B is given by:

$$P_{\mathrm{B,Folded}} = \frac{[\mathrm{N}] + [\mathrm{H_2}]}{[\mathrm{N}] + [\mathrm{H_1}] + [\mathrm{H_2}] + [\mathrm{U}]} = \frac{1 + K_{\mathrm{I}}\varphi_{\mathrm{int}}}{1 + K_{\mathrm{II}}\varphi_{\mathrm{int}} + K_{\mathrm{I}}\varphi_{\mathrm{int}} + K_{\mathrm{I}}K_{\mathrm{II}}\varphi_{\mathrm{int}}}.$$

Here, [N] and [U] represent the concentrations of the native and completely unfolded proteins, respectively. [H_1] and [H_2] correspond to partially unfolded proteins with folded binding sites I and II, respectively. We have also defined the following symbols following Hilser and Thompson:

$$K_{\mathrm{II}} = \exp\left(-\frac{\Delta G_{\mathrm{II}}}{RT}\right), K_{\mathrm{I}} = \exp\left(-\frac{\Delta G_{\mathrm{I}}}{RT}\right), \varphi_{\mathrm{int}} = \exp\left(-\frac{\Delta g_{\mathrm{int}}}{RT}\right).$$

The existence of ligand A introduces additional states [N′] and [H_1'], which correspond to states N and H_1, respectively, bound by ligand A. Then, in the presence of ligand A, the probability of having a folded binding site for ligand B is shifted, as given by

$$P_{\mathrm{B,Folded}} = \frac{[\mathrm{N}] + \left[\mathrm{N}'\right] + [\mathrm{H_2}]}{[\mathrm{N}] + \left[\mathrm{N}'\right] + [\mathrm{H_1}] + \left[\mathrm{H}_1'\right] + [\mathrm{H_2}] + [\mathrm{U}]} = \frac{1 + K_{\mathrm{a}}[\mathrm{A}] + K_{\mathrm{I}}\varphi_{\mathrm{int}}}{(1 + K_{\mathrm{a}}[\mathrm{A}])(1 + K_{\mathrm{II}}\varphi_{\mathrm{int}}) + K_{\mathrm{I}}\varphi_{\mathrm{int}} + K_{\mathrm{I}}K_{\mathrm{II}}\varphi_{\mathrm{int}}},$$

where K_{a} is the intrinsic association constant for ligand A. This is the definition of allostery in their paper. They next investigated when such a shift is maximized.

Now, let us assume that the abovementioned protein is an EF-SAM dimer and both ligands A and B are identified as Ca^{2+}. For simplicity, we will assume it to be a symmetric dimer so that it has two identical Ca^{2+}-binding cEF-hands with the same intrinsic association constant K_{a}, and $K_{\mathrm{unfold}} \equiv K_{\mathrm{I}} = K_{\mathrm{II}}$. This assumption simplifies the mathematics but does not affect the result qualitatively. Then, we can express the concentration of each state in terms of the concentration of native protein, [N], as in the following table:

	No. of bound Ca^{2+}	State	Ratio to [N]
[N]	0	Native	1
[N′]	1	Native	$2\,K_a[Ca^{2+}]$
[N″]	2	Native	$(K_a[Ca^{2+}])^2$
[H]	0	Partially unfolded	$2\,K_{unfold}\varphi_{int}$
[H′]	1	Partially unfolded	$2\,K_a[Ca^{2+}]K_{unfold}\varphi_{int}$
[U]	0	Completely unfolded	$K^2_{unfold}\varphi_{int}$

Note that [N′], [H], and [H′] acquire an extra factor of 2 because both binding site I and II contribute and K_a is defined for each binding site separately. Now, if we could ignore the dissociation of the dimer (which of course we cannot when our focus is on the monomer fraction), the fraction of Ca^{2+}-bound sites could be expressed as:

$$P_{occupied} = \frac{\#\text{of occupied binding sites}}{\#\text{of total binding sites}} = \frac{[N'] + 2[N''] + [H']}{2[N] + 2[N'] + 2[N''] + 2[H] + 2[H'] + 2[U]}$$

$$= \frac{K_a\left[Ca^{2+}\right] + \left(K_a\left[Ca^{2+}\right]\right)^2 + K_a\left[Ca^{2+}\right]K_{unfold}\varphi_{int}}{1 + 2K_a\left[Ca^{2+}\right] + \left(K_a\left[Ca^{2+}\right]\right)^2 + 2K_{unfold}\varphi_{int} + 2K_a\left[Ca^{2+}\right]K_{unfold}\varphi_{int} + K^2_{unfold}\varphi_{int}}.$$

The quadratic term in the numerator indicates that this quantity shows cooperative dependence on Ca^{2+} when dissociation of the dimer is not considered. However, note also that the degree of cooperativity is at most quadratic, just as in the simpler model in the text, where the fraction of Ca^{2+}-bound sites is given by:

$$P_{occupied} = \frac{[D'] + 2[D'']}{2[D] + 2[D'] + 2[D'']} = \frac{K'_a\left[Ca^{2+}\right] + 2K'_aK''_a\left[Ca^{2+}\right]^2}{2 + 2K'_a\left[Ca^{2+}\right] + 2K'_aK''_a\left[Ca^{2+}\right]^2}$$

These results imply that the addition of distinguishable unfolded states does not increase the degree of cooperativity beyond that of the simpler model.

For a more realistic calculation, we would have to include the dissociation of the dimer. Instead of performing this calculation explicitly, we will simply make an analogy with the abovementioned calculation. The resultant expression of K_d with additional distinguishable unfolded states contains a quadratic term in its numerator as in the abovementioned expression of the fraction of Ca^{2+}-bound sites. However, this is again the same result we obtained for K_d using the simpler model; that is, the inclusion of additional unfolded states does not qualitatively affect the degree of cooperativity in K_d. Therefore, we must reach the same conclusion as in the simpler model; namely, the monomer fraction is at most linear after we consider the dissociation of the dimer. In other words, the cooperativity with respect to $[Ca^{2+}]$ in the fraction of Ca^{2+}-bound sites does not imply cooperativity in the monomer fraction. Since it is the later quantity that was observed to behave cooperatively with respect to $[Ca^{2+}]$, we must look elsewhere for an explanation of this behavior.

Received 3 November 2013;
Received in revised form 10 February 2014;
Accepted 12 March 2014
Available online 17 March 2014

Keywords:
store-operated calcium entry;
intrinsic disorder;
STIM1;
cooperativity

†Y.F. and S.T. contributed equally to this work.
‡http://sysimm.ifrec.osaka-u.ac.jp/surFit/.

Abbreviations used:
STIM, stromal interaction molecule; IDD, intrinsically disordered domain; PPI, protein–protein interaction;

ER, endoplasmic reticulum; SOCE, store-operated Ca^{2+} entry; PM, plasma membrane; CRAC, Ca^{2+} release activated Ca^{2+}; AUC, analytical ultracentrifugation; HSQC, heteronuclear single-quantum correlation; MD, molecular dynamics; DMD, discrete molecular dynamics.

References

[1] Dyson HJ, Wright PE. Intrinsically unstructured proteins and their functions. Nat Rev Mol Cell Biol 2005;6:197–208.

[2] Haynes C, Oldfield CJ, Ji F, Klitgord N, Cusick ME, Radivojac P, et al. Intrinsic disorder is a common feature of hub proteins from four eukaryotic interactomes. PLoS Comput Biol 2006;2:e100.

[3] Dunker AK, Cortese MS, Romero P, Iakoucheva LM, Uversky VN. Flexible nets. The roles of intrinsic disorder in protein interaction networks. FEBS J 2005;272:5129–48.

[4] Mitrea DM, Kriwacki RW. Regulated unfolding of proteins in signaling. FEBS Lett 2013;587:1081–8.

[5] Ferreon AC, Ferreon JC, Wright PE, Deniz AA. Modulation of allostery by protein intrinsic disorder. Nature 2013;498:390–4.

[6] Freiburger LA, Baettig OM, Sprules T, Berghuis AM, Auclair K, Mittermaier AK. Competing allosteric mechanisms modulate substrate binding in a dimeric enzyme. Nat Struct Mol Biol 2011;18:288–94.

[7] Garcia-Pino A, Balasubramanian S, Wyns L, Gazit E, De Greve H, Magnuson RD, et al. Allostery and intrinsic disorder mediate transcription regulation by conditional cooperativity. Cell 2010;142:101–11.

[8] Reichheld SE, Yu Z, Davidson AR. The induction of folding cooperativity by ligand binding drives the allosteric response of tetracycline repressor. Proc Natl Acad Sci U S A 2009;106:22263–8.

[9] Hilser VJ, Thompson EB. Intrinsic disorder as a mechanism to optimize allosteric coupling in proteins. Proc Natl Acad Sci U S A 2007;104:8311–5.

[10] Reichmann D, Jakob U. The roles of conditional disorder in redox proteins. Curr Opin Struct Biol 2013;23:436–42.

[11] Baba Y, Nishida K, Fujii Y, Hirano T, Hikida M, Kurosaki T. Essential function for the calcium sensor STIM1 in mast cell activation and anaphylactic responses. Nat Immunol 2008;9:81–8.

[12] Oh-Hora M, Yamashita M, Hogan PG, Sharma S, Lamperti E, Chung W, et al. Dual functions for the endoplasmic reticulum calcium sensors STIM1 and STIM2 in T cell activation and tolerance. Nat Immunol 2008;9:432–43.

[13] Matsumoto M, Fujii Y, Baba A, Hikida M, Kurosaki T, Baba Y. The calcium sensors STIM1 and STIM2 control B cell regulatory function through interleukin-10 production. Immunity 2011;34:703–14.

[14] Stiber J, Hawkins A, Zhang ZS, Wang S, Burch J, Graham V, et al. STIM1 signalling controls store-operated calcium entry required for development and contractile function in skeletal muscle. Nat Cell Biol 2008;10:688–97.

[15] Picard C, McCarl CA, Papolos A, Khalil S, Luthy K, Hivroz C, et al. STIM1 mutation associated with a syndrome of immunodeficiency and autoimmunity. N Engl J Med 2009;360:1971–80.

[16] Stathopulos PB, Zheng L, Li GY, Plevin MJ, Ikura M. Structural and mechanistic insights into STIM1-mediated initiation of store-operated calcium entry. Cell 2008;135:110–22.

[17] Stathopulos PB, Li GY, Plevin MJ, Ames JB, Ikura M. Stored Ca^{2+} depletion-induced oligomerization of stromal interaction molecule 1 (STIM1) via the EF-SAM region: an initiation mechanism for capacitive Ca^{2+} entry. J Biol Chem 2006;281:35855–62.

[18] Yang X, Jin H, Cai X, Li S, Shen Y. Structural and mechanistic insights into the activation of stromal interaction molecule 1 (STIM1). Proc Natl Acad Sci U S A 2012;109:5657–62.

[19] Zhou Y, Srinivasan P, Razavi S, Seymour S, Meraner P, Gudlur A, et al. Initial activation of STIM1, the regulator of store-operated calcium entry. Nat Struct Mol Biol 2013;20:973–81.

[20] Soboloff J, Rothberg BS, Madesh M, Gill DL. STIM proteins: dynamic calcium signal transducers. Nat Rev Mol Cell Biol 2012;13:549–65.

[21] Hogan PG, Lewis RS, Rao A. Molecular basis of calcium signaling in lymphocytes: STIM and ORAI. Annu Rev Immunol 2010;28:491–533.

[22] Brandman O, Liou J, Park WS, Meyer T. STIM2 is a feedback regulator that stabilizes basal cytosolic and endoplasmic reticulum Ca^{2+} levels. Cell 2007;131:1327–39.

[23] Luik RM, Wang B, Prakriya M, Wu MM, Lewis RS. Oligomerization of STIM1 couples ER calcium depletion to CRAC channel activation. Nature 2008;454:538–42.

[24] McRorie DK, Voelker PJ. Self-associating systems in the analytical ultracentrifuge. Palo Alto: Beckman Instruments, Inc.; 1993.

[25] Kumar S, Rosenberg JM, Bouzida D, Swendsen RH, Kollman PA. THE weighted histogram analysis method for free-energy calculations on biomolecules. I. The method. J Comput Chem 1992;13:1011–21.

[26] Zheng L, Stathopulos PB, Li GY, Ikura M. Biophysical characterization of the EF-hand and SAM domain containing Ca^{2+} sensory region of STIM1 and STIM2. Biochem Biophys Res Commun 2008;369:240–6.

[27] Ward JJ, McGuffin LJ, Bryson K, Buxton BF, Jones DT. The DISOPRED server for the prediction of protein disorder. Bioinformatics 2004;20:2138–9.

[28] Schellman JA. The thermodynamics of solvent exchange. Biopolymers 1994;34:1015–26.

[29] Myers JK, Pace CN, Scholtz JM. Denaturant m values and heat capacity changes: relation to changes in accessible surface areas of protein unfolding. Protein Sci 1995;4:2138–48.

[30] Guharoy M, Chakrabarti P. Secondary structure based analysis and classification of biological interfaces: identification of binding motifs in protein–protein interactions. Bioinformatics 2007;23:1909–18.

[31] Oliveberg M, Wolynes PG. The experimental survey of protein-folding energy landscapes. Q Rev Biophys 2005;38:245–88.

[32] Heidarsson PO, Otazo MR, Bellucci L, Mossa A, Imparato A, Paci E, et al. Single-molecule folding mechanism of an EF-hand neuronal calcium sensor. Structure 2013;21:1812–21.

[33] Gunasekaran K, Ma B, Nussinov R. Is allostery an intrinsic property of all dynamic proteins? Proteins 2004;57:433–43.

[34] Lewit-Bentley A, Rety S. EF-hand calcium-binding proteins. Curr Opin Struct Biol 2000;10:637–43.

[35] Zheng L, Stathopulos PB, Schindl R, Li GY, Romanin C, Ikura M. Auto-inhibitory role of the EF-SAM domain of STIM proteins in store-operated calcium entry. Proc Natl Acad Sci U S A 2011;108:1337–42.

[36] Schuhmann MK, Stegner D, Berna-Erro A, Bittner S, Braun A, Kleinschnitz C, et al. Stromal interaction molecules 1 and 2 are key regulators of autoreactive T cell activation in murine autoimmune central nervous system inflammation. J Immunol 2010;184:1536–42.

[37] McCarl CA, Khalil S, Ma J, Oh-hora M, Yamashita M, Roether J, et al. Store-operated Ca^{2+} entry through ORAI1 is critical for T cell-mediated autoimmunity and allograft rejection. J Immunol 2010;185:5845–58.
[38] Greenfield NJ. Using circular dichroism spectra to estimate protein secondary structure. Nat Protoc 2006;1:2876–90.
[39] Dokholyan NV, Buldyrev SV, Stanley HE, Shakhnovich EI. Discrete molecular dynamics studies of the folding of a protein-like model. Folding Des 1998;3:577–87.
[40] Shirvanyants D, Ding F, Tsao D, Ramachandran S, Dokholyan NV. Discrete molecular dynamics: an efficient and versatile simulation method for fine protein characterization. J Phys Chem B 2012;116:8375–82.
[41] Ding F, Tsao D, Nie H, Dokholyan NV. Ab initio folding of proteins with all-atom discrete molecular dynamics. Structure 2008;16:1010–8.
[42] Dagliyan O, Proctor EA, D'Auria KM, Ding F, Dokholyan NV. Structural and dynamic determinants of protein–peptide recognition. Structure 2011;19:1837–45.
[43] Fukunishi Y, Mikami Y, Nakamura H. Similarities among receptor pockets and among compounds: analysis and application to *in silico* ligand screening. J Mol Graphics Modell 2005;24:34–45.